Hindawi Publishing Corporation
Journal of Nanomaterials
Volume 2013, Article ID 181543, 7 pages
http://dx.doi.org/10.1155/2013/181543

Research Article

Heat Transfer between an Individual Carbon Nanotube and Gas Environment in a Wide Knudsen Number Regime

Hai-Dong Wang,[1] Jin-Hui Liu,[1] Xing Zhang,[1] Tian-Yi Li,[2] Ru-Fan Zhang,[3] and Fei Wei[3]

[1] *Key Laboratory for Thermal Science and Power Engineering of Ministry of Education, Department of Engineering Mechanics, Tsinghua University, Beijing 100084, China*
[2] *Department of Physics and Tsinghua-Foxconn Nanotechnology Research Center, Tsinghua University, Beijing 100084, China*
[3] *Beijing Key Laboratory of Green Chemical Reaction Engineering and Technology, Department of Chemical Engineering, Tsinghua University, Beijing 100084, China*

Correspondence should be addressed to Xing Zhang; x-zhang@tsinghua.edu.cn

Received 14 March 2013; Accepted 20 May 2013

Academic Editor: Teng Li

Applications of carbon nanotube (CNT) and graphene in thermal management have recently attracted significant attention. However, the lack of efficient prediction formula for heat transfer coefficient between nanomaterials and gas environment limits the further development of this technique. In this work, a kinetic model has been established to predict the heat transfer coefficient of an individual CNT in gas environment. The heat dissipation around the CNT is governed by molecular collisions, and outside the collision layer, the heat conduction is dominant. At nanoscales, the natural convection can be neglected. In order to describe the intermolecular collisions around the CNT quantitatively, a correction factor 1/24 is introduced and agrees well with the experimental observation. The prediction of the present model is in good agreement with our experimental results in free molecular regime. Further, a maximum heat transfer coefficient occurs at a critical diameter of several nanometers, providing guidelines on the practical design of CNT-based heat spreaders.

1. Introduction

As the scale of electronic devices continuously decreases to nanometers, the power density increases to a very high level; for example, an individual microprocessor operating at a low GHz frequency has a typical power density of 100 Wcm^{-2} [1]. Meanwhile, the waste heat at this high generation rate has to be dissipated efficiently in a limited space; otherwise, the resulting local high temperature may cause thermal failure of the device and highly reduce its lifetime. Hence, the thermal management at nanoscales has become a critical issue and attracted much attention. Recently, the carbon nanotube (CNT), nanowires, and graphene have been found to be the promising materials to remove the waste heat from nanoelectronic devices due to their super high thermal conductivities [2–5]. At two-dimensional scales, the graphene has important applications as heat spreaders and thermal interfacial materials [6–8]. Meanwhile, the CNT can be designed into a one-dimensional heat spreader connecting the hotspot with high power density and the heat sinks. These new techniques have potential applications in many areas, such as nanoelectromechanical systems [9], gas sensors [10], field emitters [11], and nanowire-based lasers [12, 13]. Since all the nanodevices will be used in the air environment, the study of heat transfer between the nanomaterials and surrounding air forms the foundation of the practical design of nano heat spreaders.

Heat transfer across the interface between macroscale solid and gas environment is well understood, where many experimental data and empirical formulas are available. However, as the characteristic size scales down to nanometers, it becomes a challenging task to determine the heat transfer coefficient (HTC) of nanomaterials quantitatively. In the experimental study, the commonly used resistance thermometer or thermocouples at macroscales are no longer applicable, and a noncontact measurement should be performed at the nanometer level in order to avoid the uncertainty of temperature measurement at interfaces. Recently,

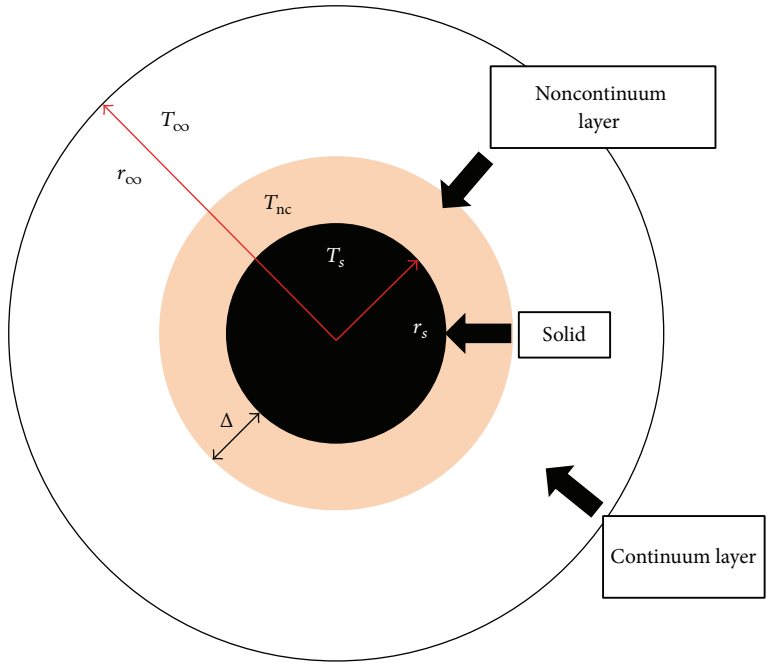

Figure 1: Schematic diagram of the two-layer model.

a noncontact technique of micro-Raman spectroscopy has been utilized to measure the thermal properties of CNT and graphene [9, 10, 14–16]. In this technique, a focused laser is used to heat the sample locally and the temperature response can be measured simultaneously from the downshifted G-band frequency. Combining with electrical measurement, both the optical absorption and thermal conductivity of an individual CNT can be obtained [16]. While this technique has the potential to provide both thermal conductivity and HTC of an individual CNT, the presented experimental data are still too few to conclude a convincing variation trend of the thermal property on a single parameter of CNT, like its length, diameter, or chirality.

In the theoretical study, no quantitative theoretical model has been fully developed to predict the HTC between an individual CNT and gas environment. Some molecular dynamics (MD) simulations of CNT-air interfacial thermal conductance have been reported and give a result of about 1.0×10^5 $\mathrm{Wm^{-2}\,K^{-1}}$ [17]. The associated thermal resistance is equivalent to the resistance of about 250 nm thick layer of air. Because of the high surface to volume ratios, the heat dissipation from an individual CNT to the gas environment becomes increasingly important compared with that at macroscales [5]. The heat dissipated across the CNT-air interface is more than 50% for a 2.04 nm, 5 μm long suspended CNT [18], and this fraction will approach 100% for CNTs longer than 60 μm [19]. Hence, the heat dissipation to the air environment can be exploited as an effective way for cooling CNT associated devices [20]. It is particularly important to develop an accurate prediction model for the HTC of individual CNT or nanowire, benefiting the practical thermal design of efficient heat spreaders at nanoscales. On the other hand, from CNT to nanowire, the characteristic diameter of HTC changes from several nanometers to hundreds of nanometers, ranging from the free molecular regime to the transition regime. The development of a unified theoretical model also has important academic significance.

In this work, a theoretical model of heat transfer across the CNT-gas interface has been established based on the kinetic theory. It demonstrates that a critical diameter exists at several nanometers for a maximum HTC of 1.08×10^5 $\mathrm{Wm^{-2}\,K^{-1}}$. The theoretical prediction agrees well with our experimental results in the free molecular regime [19].

2. Two-Layer Model of Heat Transfer

Fuchs proposed a general physical model to estimate the heat transfer between the gas environment and isolated particle at submicroscales [21, 22]. In this model, the whole space is separated into two layers: the layer around the particle with a thickness comparable to the mean free path (MFP) of molecules and the outside layer where the continuum theory is applicable. A schematic diagram of this two-layer model is shown in Figure 1.

Figure 1 shows the two-layer model for a spherical particle. The black circle in the center represents the solid part, around which a thin layer is the noncontinuum layer with a thickness of Δ. T_s, T_{nc}, and T_∞ are the temperatures at the solid surface and at the interface of noncontinuum layer and of surrounding gas, respectively. r_s and r_∞ are the radiuses of solid particle and outer continuum layer when $T = T_\infty$, respectively. In this model, the heat transfer from the solid surface to the outer gas environment is finished in two steps: (1) energy exchange between the solid surface and gas molecules by collisions in the noncontinuum layer; (2) heat dissipation in the outer continuum layer. In Fuchs' model,

the first step heat transfer is described by molecular kinetics and the second step is described by means of continuum theory. Following this model, a governing equation for the HTC between the nanoparticles and surrounding gas is given as [23]

$$h = \frac{Q}{4\pi r_s^2 (T_s - T_\infty)} = \frac{\lambda f_{\text{ncr}} (\xi + \gamma)}{l \left[f_{\text{ncr}} \xi^2 + \beta (\xi + \gamma) \right]}, \quad (1)$$

where h, Q, λ, and l are the heat coefficient, heat dissipated into the gas environment, thermal conductivity of gas, and molecular MFP, respectively; $\xi = r_s/l$ is the dimensionless radius, and $\gamma = \Delta/l$ is the dimensionless thickness of inner layer. $f_{\text{ncr}} = \xi[1 + \xi e^{\xi} \text{Ei}(-\xi)]$ is the correction factor in the noncontinuum layer, where $\text{Ei}(x)$ is the exponential integral of x. β is the correction factor for molecular collisions.

Based on (1), the Nusselt number Nu can be summarized as

$$\text{Nu} = \frac{2r_s h}{\lambda} = \frac{2 f_{\text{ncr}} \xi (\xi + \gamma)}{f_{\text{ncr}} \xi^2 + \beta (\xi + \gamma)}. \quad (2)$$

This two-layer model is capable of predicting the HTC of particle with a diameter ranging from nanometers to micrometers, and the corresponding Knudsen number Kn is from 0.01 to 10. However, some questions still remain to limit the prediction accuracy: (1) an exact equivalent particle radius is needed for a good prediction, which is usually hard to get for aerosolized nanoparticles; (2) the molecular motion inside the inner layer is considered to be collisionless and there is no transition layer between the two layers in Figure 1 [24]. Ignoring the interactions between molecules may cause prediction uncertainty. Reference [23] takes into account the intermolecular collisions by changing the inner layer thickness and this thickness is assumed to increase as the particle diameter increases. But the accurate inner layer thickness is difficult to evaluate in practical applications.

In this work, we developed a prediction formula for the HTC of an individual CNT based on the two-layer model. The physical model shown in Figure 1 is applicable using a cylindrical coordinate system instead. The noncontinuum layer is adjacent to the CNT surface, where the kinetic theory is applied. The outside continuum layer is concentric with the CNT and the noncontinuum layer, where the continuum theory is applied. In the noncontinuum layer, the average velocity of molecules is given as [25]

$$\bar{v} = 2\left(\frac{2k_B T}{\pi m} \right)^{1/2}, \quad (3)$$

where k_B and m are the Boltzmann constant and mass of a molecule, respectively. In a cylindrical coordinate system, the number of molecules moving towards the solid surface with an incident angle θ is givens as

$$N = nr\,\text{d}\theta\,\text{d}r\,\text{d}x \frac{\cos\theta\,\text{d}s}{2\pi r L}, \quad (4)$$

where n, r, L, and ds are the molecular number density, radius, CNT length, and area element, respectively. Using the classical Maxwell distribution function, the fraction of molecules with a velocity between v and dv is given as

$$N_{\text{d}v} = 4\pi \left(\frac{m}{2\pi k_B T} \right)^{3/2} v^2 \exp\left(-\frac{mv^2}{2k_B T} \right) \text{d}v. \quad (5)$$

The molecular impact flux on the solid surface is given as [23]

$$\begin{aligned} \psi &= \frac{2mn}{\pi^2 k_B T l} \int_0^\infty \left(\frac{r_s}{r_s + \Delta} \right)^2 \exp\left(\frac{-\Delta}{l} \right) \text{d}\Delta \\ &\quad \times \int_0^\infty v^2 \exp\left(-\frac{mv^2}{2k_B T} \right) \text{d}v \\ &= \frac{\bar{v}n}{2\pi} \xi \left[1 + \xi e^{\xi} \text{Ei}(-\xi) \right] = \frac{\bar{v}n}{2\pi} f_{\text{ncr}}. \end{aligned} \quad (6)$$

The dissipated energy Q at the wire surface can be described as

$$Q = \psi S \alpha_f C_v m (T_s - T_{\text{nc}}). \quad (7)$$

Substituting the integrated result of ψ into (7), one can get

$$Q = 2\alpha_f d L n C_v m f_{\text{ncr}} \sqrt{\frac{k_B T}{2\pi m}} (T_s - T_{\text{nc}}), \quad (8)$$

where S, α_f, C_v, T_s, T_{nc}, and d are the wire surface, accommodation coefficient, specific heat capacity at constant volume, solid surface temperature, noncontinuum layer temperature, and diameter of CNT, respectively.

According to the kinetic theory of gas, the thermal conductivity is given as [26]

$$\lambda = \frac{2\beta'}{\pi} \frac{\bar{v}n}{4} C_v m l = \beta n C_v m l \sqrt{\frac{k_B T}{2\pi m}}, \quad (9)$$

where l is the molecular MFP and β is the correction factor representing the effect of intermolecular collisions. The constant $2/\pi$ is caused by the different geometric coordinates of cylinder and sphere. Combining (8) and (9), the heat flux from the CNT surface to the noncontinuum layer is derived as

$$q_{s-\text{nc}} = \alpha_f \frac{\lambda f_{\text{ncr}}}{\beta l} (T_s - T_{\text{nc}}). \quad (10)$$

Figure 2 shows a schematic diagram of molecular collisions around an individual CNT. Because the diameter of CNT is much smaller than the molecular MFP, the probability of molecules colliding with CNT decreases as the diameter decreases. In this case, the surrounding gas appears to be rarefied for the CNT. As shown in Figure 2, the CNT is "covered" by a layer of molecules with a thickness of molecular MFP, referred to as the noncontinuum layer. Out of this layer, the gas is continuous and the collision cross-section is given as $\sigma = \pi l^2$. To consider the probability that a molecule appears in the volume of CNT with a diameter of d, the cross-section is given as $\sigma_{\text{CNT}} = 0.25\pi d^2$. $\sigma_{\text{CNT}}/\sigma$ equals zero as the diameter approaches zero, and it equals

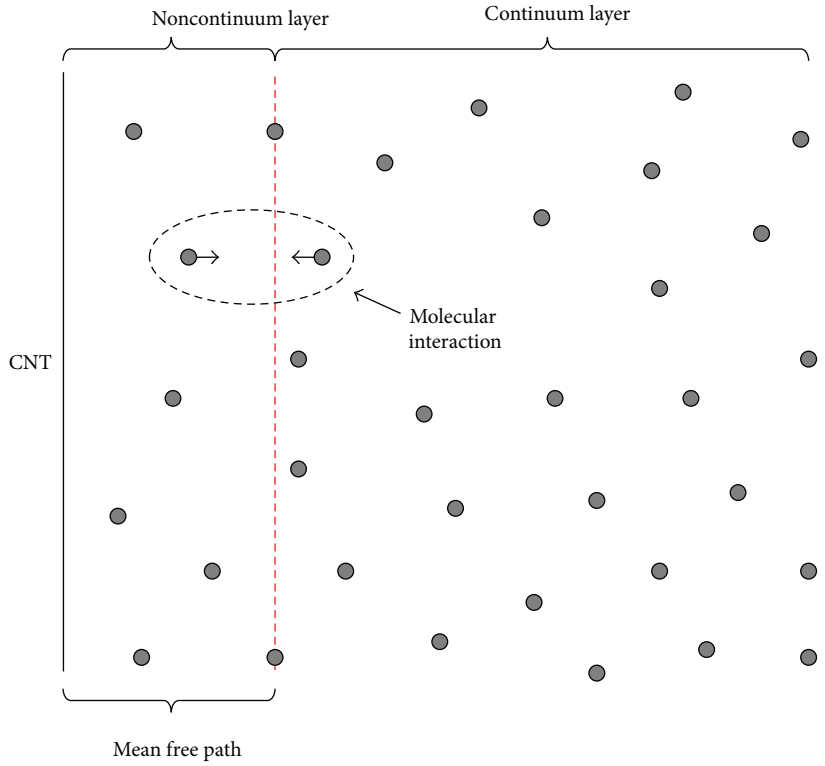

Figure 2: Schematic diagram of molecular collision model.

unity as the radius of CNT approaches the molecular MFP. The integration average value of $\sigma_{\mathrm{CNT}}/\sigma$ from zero to l equals 1/3. On the other hand, the reflected molecules from the CNT surface will collide with the other incident molecules within the layer of MFP, and the molecular interaction will decrease the collision probability. If every reflected molecule collides with the incoming one, that gives a limiting value of 1/2 for each direction. In a three-dimensional space, this fraction is 1/8. As a result, the correction factor β can be estimated as about 1/24.

In the continuum layer, the hear flux caused by heat conduction from radius r_1 to radius r_2 is $q = (\lambda/r_s)\Delta T/\ln(r_2/r_1)$, where r_s is the solid wire radius. The heat conductance $q/\Delta T$ is inversely proportional to the radius r_s. When $r_w = 2\,\mu$m, the HTC of natural convection is about $3.4 \times 10^3\ \mathrm{Wm^{-2}\,K^{-1}}$ [26, 27], while the heat conductance $q/\Delta T$ is about $1.4 \times 10^4\ \mathrm{Wm^{-2}\,K^{-1}}$, and the most heat is dissipated by conduction. As the radius r_s decreases to submicrometers, the Grashof number Gr decreases rapidly below 1×10^{-7} in the third power of radius, implying that the buoyancy force is negligible compared with the viscous force and the heat conduction becomes the only dominant way. Governed by the one-dimensional heat conduction equation in cylindrical coordinates, the heat flux from the noncontinuum layer to the gas environment is given as

$$q_{\mathrm{nc}-\infty} = \frac{\lambda}{r_s + \Delta}\left(\frac{T_{\mathrm{nc}} - T_\infty}{\ln\left(n_r\left(r_s + r_0\right)/\left(r_s + \Delta\right)\right)}\right), \quad (11)$$

where T_∞ is the environment temperature and $r_\infty = n_r(r_w + r_0)$ is the radius when $T = T_\infty$. Imposing the continuity condition on heat flux at the interface between noncontinuum layer and continuum layer, the temperature T_{nc} is given as

$$T_{\mathrm{nc}} = T_s - \left[1 + \frac{f_{\mathrm{ncr}}}{\beta l}\left(r_s + \Delta\right)\ln\left(\frac{r_\infty}{r_s + \Delta}\right)\right]^{-1}\left(T_s - T_\infty\right). \quad (12)$$

Hence, we derived the HTC h as

$$h = \frac{Q}{\pi d L\left(T_s - T_\infty\right)} = \frac{(2/\pi)\,\alpha_f n C_v m f_{\mathrm{ncr}}\sqrt{k_B T/2\pi m}}{1 + \left(f_{\mathrm{ncr}}/\beta l\right)\left(r_s + \Delta\right)\ln\left(n_r\left(\left(r_s + r_0\right)/\left(r_s + \Delta\right)\right)\right)}. \quad (13)$$

3. Results and Discussion

In order to verify the accuracy of the present theoretical model, we measured the HTCs of several single-walled CNTs (SWCNTs) using a Raman spectroscopy technique [19]. The experimental data and theoretical predictions are compared in Figure 3.

As shown in Figure 3, the experimental data (red circles) match quite well the present model (solid curve) in a diameter range from 0.97 nm to 1.47 nm. Meanwhile, the literature data of microwires agree well with the present model as well [26]. When the accommodation coefficient α_f equals unity, the maximum value of h is given as [28]

$$h_{\max} = \frac{5}{8} n u k_B = 1.1 \times 10^5\ \mathrm{Wm^{-2}\,K^{-1}}, \quad (14)$$

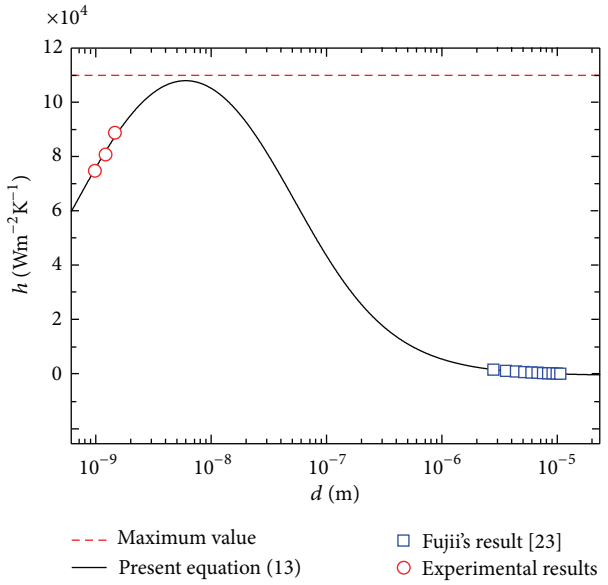

Figure 3: Comparison between the experimental data and theoretical prediction. The red dash line is the maximum value given by the kinetic theory.

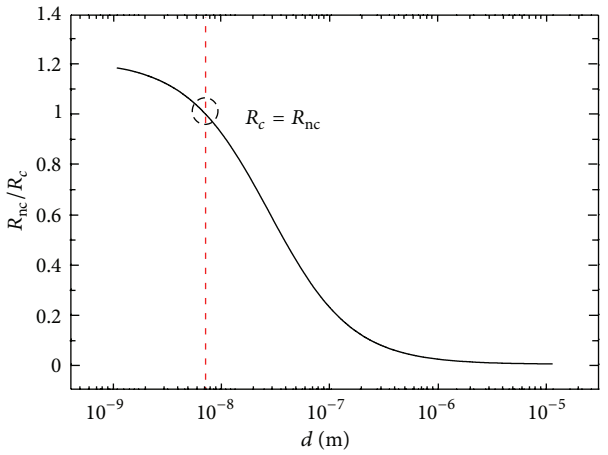

Figure 4: Ratio between the thermal resistances of noncontinuum and continuum layers plotted with respect to the diameter. The red dash line marks the critical diameter when $R_{nc} = R_c$.

where $u = (3k_BT/m)^{0.5}$ is the root mean square velocity. The maximum value predicted by (13) is 1.08×10^5 Wm^{-2} K^{-1}, consistent with the prediction of (14). The best fitted parameters for the calculation result of Figure 3 are $\alpha_f = 1$, $\beta = 0.04$, $n_r = 100$, and $r_0 = 0.4l$. As mentioned previously, the correction factor β can be calculated as

$$\beta = \frac{1}{8}\int_0^{2l} \frac{\sigma}{\sigma_{CNT}} dx = \frac{1}{8}\int_0^{2l} \frac{\pi x^2}{4\pi l^2} dx = \frac{1}{24} \approx 0.04, \quad (15)$$

and the best fitted value is consistent with the theoretical prediction, showing a good accuracy of the present model.

Figure 4 shows the ratio between the thermal resistances of noncontinuum layer and continuum layer, that is, R_{nc} and R_c, respectively. Here, the previous thermal resistance is calculated as $R_{nc} = l/\lambda$, where the thermal conductivity λ is calculated by (9) containing the correction factor β. The latter thermal resistance is calculated as $R_c = (r_\infty/\lambda_{air}) \ln [r_\infty/(r_s + l)]$, where the thermal conductivity of air λ_{air} is used. It is seen in Figure 4 that the continuum layer contributes to the most thermal resistance when the diameter is at micrometers; in this case, the noncontinuum layer around the thin wire can be totally neglected. However, as the diameter decreases, the resistance R_{nc} becomes more and more important and the difference between R_{nc} and R_c decreases rapidly below 100 nm. At a critical diameter of about 5 nm, R_{nc} equals R_c and a maximum HTC value occurs as shown in Figure 3. When the diameter drops below the critical value, R_{nc} becomes larger than R_c and the HTC decreases as well. As a result, the existence of a maximum HTC is caused by the competition between R_{nc} and R_c.

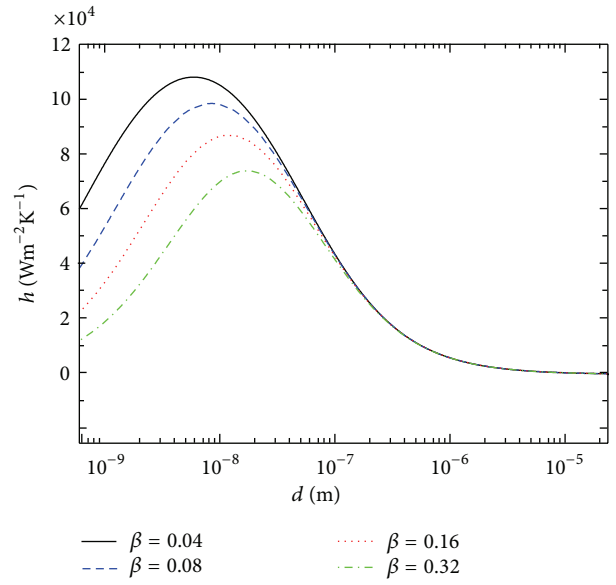

Figure 5: The effect of molecular interactions on the HTC.

Figure 5 shows the HTC predicted by (13) with a correction factor β changing from 0.04 to 0.32. For a given temperature difference $T_s - T_{nc}$, the dissipated heat Q is proportional to the molecular number density n based on (8). As the correction factor β increases, the probability of intermolecular collisions inside the noncontinuum layer increases and the effective molecular density decreases. Thus the dissipated heat Q decreases and HTC h decreases as well. Changing the factor β only affects the HTC with a diameter below 100 nm, and the results of thick wires remain unchanged.

Based on (13), a dimensionless Nusselt number Nu is given as

$$\mathrm{Nu} = \frac{hd}{\lambda} = \frac{4\alpha_f f_{ncr} \xi/\pi}{\beta + f_{ncr}(\xi + \Delta/l) \ln\left(n_r\left((\xi + r_0/l)/(\xi + \Delta/l)\right)\right)}. \quad (16)$$

The calculation results of (16) are given in Figure 6 as follows.

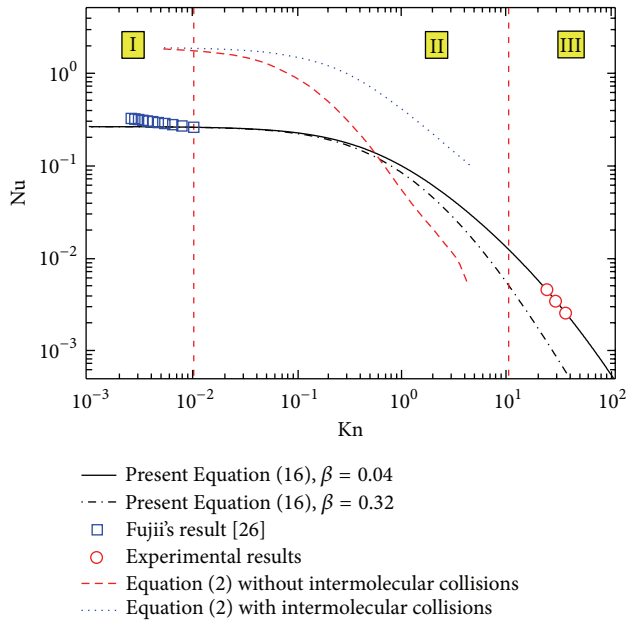

Figure 6: Nusselt number plotted with respect to Knudsen's number, and different values of factor β are used for calculation. The regimes I, II, and III are the continuum regime, transition regime, and free molecular regime, respectively.

In Figure 6, the black solid and dash-dot curves are the prediction results of the present model for CNTs. The red dash curve and blue dot curve are the prediction results for nanoparticles, where the previous one takes into account the intermolecular collisions while the latter one does not [23]. Equation (2) relates the molecular interaction with the thickness of noncontinuum layer, and the increasing thickness decreases the dissipated heat at the particle surface. Similarly in the present model, as the CNT diameter increases, more molecules are reflected from the solid surface and collide with other molecules and the correction factor β increases. Using gas dynamics, the exact value of β can be estimated.

Figure 6 can be divided into three regimes, that is, the continuum regime (Kn $< 10^{-2}$), transition regime ($10^{-2} <$ Kn < 10), and free molecular regime (Kn > 10), respectively. In the continuum regime, the continuum the-ory is applicable and the thermal resistance induced by the molecular collisions at the solid surface is negligible. As the diameter decreases to the transition regime, the molecular interactions become more significant and reduce the Nu number accordingly. Finally in the free molecular regime, the intermolecular interactions within the MFP layer play a dominant role and decide the HTC. The present model given in (13) and (16) has been proved valid by the experiments in both free molecular and continuum regimes, while the experimental data in the transition regime are still lacking. In our future work, the HTC in a wide Kn number from 0.01 to 100 will be measured.

4. Summary

(1) So far, there is no efficient theoretical model proposed to predict the HTC between an individual CNT and gas environment. In this work, a quantitative model has been established to predict HTC, and the prediction of the present model is in good agreement with the experimental data in both free molecular and continuum regimes.

(2) The present model demonstrates that the natural convection can be neglected in the continuum layer outside the CNT, where the heat conduction plays a dominant role.

(3) In the previous models for nanoparticles, it is difficult to evaluate the effect of intermolecular collisions on HTC around the solid surface. In the present model, the intermolecular effect can be quantitatively calculated using a correction factor β, and the analytical value is consistent with the experimental observation.

(4) It is predicted by the present model that a maximum HTC exists in the transition regime, corresponding to a critical diameter at several nanometers. Similar to the concept of critical diameter of thermal insulation layer, the critical diameter here accounts for the dividing line of relative importance between the thermal resistances of noncontinuum layer and continuum layer. In practical applications, the performance of CNT-based heat spreader can be improved by choosing the critical diameters.

Acknowledgments

The authors would like to acknowledge the great help and support from Professor Zeng-Yuan Guo. The main idea of this work is derived from the discussion with Guo. This work is financially supported by the National Natural Science Foundation of China (Grant nos. 51076080 and 51136001), China Postdoctoral Science Foundation funded project, and Tsinghua University Initiative Scientific Research Program.

References

[1] E. Pop, "Energy dissipation and transport in nanoscale devices," *Nano Research*, vol. 3, no. 3, pp. 147–169, 2010.

[2] S. Chen, A. L. Moore, W. Cai et al., "Raman measurements of thermal transport in suspended monolayer graphene of variable sizes in vacuum and gaseous environments," *ACS Nano*, vol. 5, no. 1, pp. 321–328, 2011.

[3] P. Kim, L. Shi, A. Majumdar, and P. L. McEuen, "Thermal transport measurements of individual multiwalled nanotubes," *Physical Review Letters*, vol. 87, no. 21, Article ID 215502, 4 pages, 2001.

[4] S. V. Rotkin, V. Perebeinos, A. G. Petrov, and P. Avouris, "An essential mechanism of heat dissipation in carbon nanotube electronics," *Nano Letters*, vol. 9, no. 5, pp. 1850–1855, 2009.

[5] C. Cheng, W. Fan, J. Cao et al., "Heat transfer across the interface between nanoscale solids and gas," *ACS Nano*, vol. 5, no. 12, pp. 10102–10107, 2011.

[6] A. A. Balandin, "Thermal properties of graphene and nanostructured carbon materials," *Nature Materials*, vol. 10, no. 8, pp. 569–581, 2011.

[7] K. M. F. Shahil and A. A. Balandin, "Thermal properties of graphene and multilayer graphene: applications in thermal

interface materials," *Solid State Communications*, vol. 152, no. 15, pp. 1331–1340, 2012.

[8] D. L. Nika and A. A. Balandin, "Two-dimensional phonon transport in graphene," *Journal of Physics: Condensed Matter*, vol. 24, no. 23, Article ID 233203, 2012.

[9] R. H. Blick and M. Grifoni, "Focus on nano-electromechanical systems," *New Journal of Physics*, vol. 7, pp. 1367–2630, 2005.

[10] E. Strelcov, Y. Lilach, and A. Kolmakov, "Gas sensor based on metal-insulator transition in VO_2 nanowire thermistor," *Nano Letters*, vol. 9, no. 6, pp. 2322–2326, 2009.

[11] J. She, Z. Xiao, Y. Yang et al., "Correlation between resistance and field emission performance of individual ZnO one-dimensional nanostructures," *ACS Nano*, vol. 2, no. 10, pp. 2015–2022, 2008.

[12] M. H. Huang, S. Mao, H. Feick et al., "Room-temperature ultraviolet nanowire nanolasers," *Science*, vol. 292, no. 5523, pp. 1897–1899, 2001.

[13] L. K. van Vugt, S. Ruhle, and D. Vanmaekelbergh, "Phase-correlated nondirectional laser emission from the end facets of a ZnO nanowire," *Nano Letters*, vol. 6, no. 12, pp. 2707–2711, 2006.

[14] V. V. Deshpande, S. Hsieh, A. W. Bushmaker, M. Bockrath, and S. B. Cronin, "Spatially resolved temperature measurements of electrically heated carbon nanotubes," *Physical Review Letters*, vol. 102, no. 10, Article ID 105501, 4 pages, 2009.

[15] A. A. Balandin, S. Ghosh, W. Bao et al., "Superior thermal conductivity of single-layer graphene," *Nano Letters*, vol. 8, no. 3, pp. 902–907, 2008.

[16] I. Hsu, M. T. Pettes, A. Bushmaker, M. Aykol, L. Shi, and S. B. Cronin, "Optical absorption and thermal transport of individual suspended carbon nanotube bundles," *Nano Letters*, vol. 9, no. 2, pp. 590–594, 2009.

[17] M. Hu, S. Shenogin, P. Keblinski, and N. Raravikar, "Thermal energy exchange between carbon nanotube and air," *Applied Physics Letters*, vol. 90, no. 23, Article ID 231905, 3 pages, 2007.

[18] I. Hsu, M. T. Pettes, M. Aykol, L. Shi, and S. B. Cronin, "The effect of gas environment on electrical heating in suspended carbon nanotubes," *Journal of Applied Physics*, vol. 108, no. 8, Article ID 084307, 4 pages, 2010.

[19] H. D. Wang, L. J. Hui, Z. Y. Guo et al., "Thermal transport across the interface between a suspended single-wall carbon nanotube and air," *Nanoscale and Microscale Thermophysical Engineering*. In press.

[20] A. Beskok and G. E. Karniadakis, "A model for flows in channels, pipes, and ducts at micro and nano scales," *Microscale Thermophysical Engineering*, vol. 3, no. 1, pp. 43–77, 1999.

[21] N. A. Fuchs, "On the stationary charge distribution on aerosol particles in a bipolar ionic atmosphere," *Geofisica Pura e Applicata*, vol. 56, no. 1, pp. 185–193, 1963.

[22] N. A. Fuchs, *The Mechanics of Aerosols*, Dover, New York, NY, USA, 1989.

[23] H. H. Klein, J. Karni, R. Ben-Zvi, and R. Bertocchi, "Heat transfer in a directly irradiated solar receiver/reactor for solid-gas reactions," *Solar Energy*, vol. 81, no. 10, pp. 1227–1239, 2007.

[24] A. V. Filippov and D. E. Rosner, "Energy transfer between an aerosol particle and gas at high temperature ratios in the Knudsen transition regime," *International Journal of Heat and Mass Transfer*, vol. 43, no. 1, pp. 127–138, 2000.

[25] J. E. A. John, *Gas Dynamics*, Allyn and Bacon, Boston, Mass, USA, 1933.

[26] T. Fujii, M. Fujii, and T. Honda, "Theoretical and experimental studies of the free convection around a long horizontal thin wire in air," in *Proceedings of the 7th International Heat Transfer Conference*, vol. 2, pp. 311–316, Munich, Germany, 1982.

[27] X. Zhang, S. Fujiwara, Z. Qi, and M. Fujii, "Natural convection effect on transient short-hot-wire method," *Journal of the Japanese Society of Microgravity Applications*, vol. 16, pp. 129–135, 1999.

[28] I. K. Hsu, M. T. Pettes, M. Aykol et al., "Direct observation of heat dissipation in individual suspended carbon nanotubes using a two-laser technique," *Journal of Applied Physics*, vol. 110, no. 4, Article ID 044328, 5 pages, 2011.